Open Path Incoherent Broadband Cavity Enhanced Absorption Spectrometer for *in situ* measurement of nitrogen oxides, iodine oxide, and glyoxal in the atmosphere

Filip Pastierovič[1,2], Roberto Grilli[1], Nicolas Caillon[1], and Joel Savarino[1]

[1]Univ. Grenoble Alpes, CNRS, IRD, Grenoble INP*, IGE, F-38000 Grenoble, France
[2]Department of Experimental Physics, Faculty of Mathematics, Physics and Informatics, Comenius University, Mlynská Dolina, 842 48 Bratislava, Slovakia

Correspondence: Roberto Grilli (roberto.grilli@cnrs.fr)

Abstract. In this work we report a compact, low-cost instrument based on Open Path – Incoherent BroadBand Cavity Enhanced Absorption Spectroscopy (OP-IBBCEAS) at 445 nm for the detection of iodine oxide (IO), nitrogen oxide (NO_2) and glyoxal (CHOCHO) in the atmosphere. We provide a comparison between OP-IBBCEAS and the closed-path setup on which our

5   instrument is based, previously described in Barbero et al. 2020. The OP system achieved a noise-equivalent absorption sensitivity (NEAS) of 5.7×10^{-10} cm^{-1} $Hz^{-1/2}$ per spectral element, only 3 times higher than the closed-path system. Automated performance of regular measurements without absorbance ensures good long-term accuracy of the system. The OP-IBBCEAS is robust and simple to install in the field, allowing quantitative measurements of NO_2, CHOCHO, and IO with precisions of ±150, $\pm$ 150, and ±7 ppt (pmol mol^{-1}, 2σ) in 50 seconds of measurement.

1   Introduction

The detection and quantification of trace gases in the atmosphere is important for understanding the chemical processes that influence air quality, climate changes, Earth's radiative balance, and past climate reconstructions. Reactive species such as nitrogen oxides (NO_x = NO and NO_2), nitrate radical (NO_3) , hydroxyl, hydroperoxy and peroxy radicals (HO, HO_2, RO_2)

15   and halogen oxide radicals (XO, X = I, Br, Cl) are the main actors controlling the concentrations of the other species and working as chemical "detergents". They have significant impacts on ozone chemistry, atmospheric oxidative capacity and secondary aerosol formation, all of which have implications for both regional air quality and global climate processes Beynon and Williams (1976). In polar regions and in the marine boundary layer, halogen-containing compounds are released by biogenic and photochemical processes. The highly reactive IO radical is produced through reactions involving iodine released from sea

20   salt and organic compounds and, in combination with other halogen oxides, participates in ozone-destroying cycles, thereby impacting regional and global ozone budgets Saiz-Lopez et al. (2015), Simpson et al. (2015), Gómez Martín et al. (2020). Sim-

ilarly, NO$_2$ is a central component of atmospheric photochemistry. Alongside volatile organic compounds (VOCs), NO$_2$ is a precursor to photochemical formation of tropospheric ozone. This ground-level ozone is a major component of urban smog and poses risks to human, vegetation, and ecosystems healths. Beyond ozone formation, NO$_2$ contributes to atmospheric oxidative

25 capacity, participating in the formation of nitric acid and nitrate aerosols, which are significant components of atmospheric aerosol Romer Present et al. (2020). Glyoxal (CHOCHO) is the smallest α-dicarbonyl. It is an important intermediate in the oxidation of volatile organic compounds and contributes significantly to the secondary organic aerosols Volkamer et al. (2007). CHOCHO is not a reactive species, so can be measured in a closed-path configuration, however the presence of a particle filter in the inlet line may lead to an underestimation of its concentration in the atmosphere, as highlighted by this work.

30 Traditional measurement techniques for reactive species, particularly OH, HO$_2$, RO$_2$ and XO, are often been limited by sensitivity, spatial resolution, and the interference of surrounding gases. A further challenge is provided by the high reactivity of analyte species, and the difficulty to consistent analyte transport them into a measurement cell. Open-path configurations are generally preferred, because they avoid the sample transport problem, yet they pose other challenges related to the degradation of sensitive instrumental parts which are exposed to environmental conditions. Open-path measurements can be performed with

35 long-path differential optical absorption spectroscopy (LP-DOAS) where the measurement is integrated over few kilometres of optical path Nasse et al. (2019), Multi-Axis Differential Optical Absorption Spectroscopy (MAX-DOAS) Hönninger et al. (2004), which collects scattered sunlight at multiple angles, providing vertical profiles of trace gases, or by *in situ* instruments which provide sufficient sensitivity to detect the target species using compact optical cavities Grilli et al. (2012). MAX-DOAS is simple to build and install in the field. It is highly sensitive to absorbing gases in the lowest few kilometres of

40 the atmosphere, but the data treatment is challenging since it requires combining measurements with a radiative transfer model calculations to retrieve the vertical profiles. Unlike DOAS approaches, cavity-based instruments provide local measurements and are insensitive to meteorological conditions (clouds, foggy weather, rain, snow, etc). They are also simpler to install than LP-DOAS spectrometers because there is no need to align the beam with a distant retroreflector element.

Incoherent Broadband Cavity-Enhanced Absorption Spectroscopy (IBBCEAS) is a highly sensitive, robust, cavity-enhanced

45 absorption technique that utilizes low-cost broadband radiation to detect multiple species with high precision. The open-path configuration eliminates the need for sampling lines, avoiding losses and artifacts associated with wall interactions and secondary formation of reactive components Wang and Lu (2019). The technique allows high spatial and temporal resolution measurements, making it suitable for field applications in various environments, including urban areas and regions with moderate aerosol levels Wang and Lu (2019). Thanks to its broadband character, IBBCEAS can simultaneously monitor multiple

50 species, including HONO, NO$_2$, NO$_3$, SO$_2$, H$_2$O, IO, I$_2$, BrO, Br$_2$, O$_3$, formaldehyde (CH$_2$O) and nitrophenols Wang et al. (2023). OP-IBBCEAS has been reported to detect HONO and NO$_2$ with detection limits of 430 ppt and 1 ppb, respectively (acquisition time 90 s), Wu et al. (2012), and more recently with detection limits of 26 ppt and 76 ppt, respectively (integration time 60 s) Dixneuf et al. (2021), Dixneuf et al. (2022) . Likewise, measurements of the NO$_3$ have been made with detection limits of 36 ppt (within 10 minutes acquisition time), Suhail et al. (2019), and 3 ppt in 30 seconds were reported with an

55 effective absorption length of $\tilde{5}$ km Fanhao et al. (2022).

While OP-IBBCEAS can operate in the presence of aerosols, strong particulate matter (PM) loading can reduce sensitivity Wang and Lu (2019). In some cases, corrections for non-Beer–Lambert may be required, such as for instance the one described in Wang et al. (2023) tempting to correct the effect of strong water vapour absorption lines on the NO_3 absorption spectrum. The compact, cost-effective nature of OP-IBBCEAS makes it promising for widespread field deployments. Future developments may focus on improving the technique's robustness under strong PM loading, miniaturization and integration with other sensing technologies for comprehensive environmental monitoring Wu et al. (2012).

In this work, we present a novel open-path IBBCEAS instrument designed for simultaneous measurement of IO, NO_2 and CHOCHO. The open-path design minimizes sampling artifacts and allows for real-time measurements directly in the atmosphere, making it ideal for monitoring highly reactive and short-lived species in dynamic environments. The inlet line and the measurement cell are made of non-reactive material,so quantitative NO_2 measurements can also be made in the closed cavity. Therefore, the effort for open-path measurements provided in this work is motivated by the detection of IO and can be extended to other reactive species (BrO, ClO, OH, HO_2, RO_2, OIO, OBrO, OClO, etc). A comparison of our system with other close-path IBBCEAS setups for the detection of NO_2 is provided in Table 1 of Barbero et al. (2020). The detection limit of our system, with an effective optical path-length of 4.4 km optical path-length and an uncooled charge-coupled device (CCD) detector, was comparable with other recent developments. In the present study, a comparative analysis is presented with other open-path instruments. The characteristic performance of the existing OP-IBBCEAS for NO_2 measurements is summarised in Table 1. For the purpose of comparison, the α_{min} is used, which corresponds to the standard deviation (1 σ) of the residual of the fit. In order to have comparable values, the α_{min} is normalized by the integration time according to the following formula: $\alpha_{min} \times (t_{int})^{1/2}$, where t_{int} denotes the acquisition time of I_0 and I. By normalizing as well for the effective optical path-length we can see that the techniques reported in Table 1 ranges between 5.8×10^{-3} and 3.0×10^{-2} $Hz^{-1/2}$, and our system provide a value of 1.3×10^{-2} $Hz^{-1/2}$, which is below the average value. Depending on the acquisition time for a single acquisition, the cooling of the CCD chip may have a beneficial effect on the signal-to-noise ratio. The uncooled Avantes spectrometer used in this work for an exposure time of <200ms (as the case in this work), has a dark noise of only 0.04% of the signal, but it reaches 1% at 10 s exposure, becoming a not longer negligible source of noise. In this case, using a cooled CCD camera can reduce the dark noise by a factor of 10.

	Wavelength (nm)	Optical path-length (km)	α_{min} (cm^{-1} Hz$^{-1/2}$)	Cooled CCD
Varma et al. (2009)	630	33.5	1.73×10^{-9}	No
Wu et al. (2012)	365	2.8	1.06×10^{-7}	No
Dixneuf et al. (2022)	370	9.8	1.02×10^{-8}	Yes
Wang et al. (2023)	675	21.7	1.00×10^{-8}	Yes
This work	445	4.4	3.0×10^{-8}	No

Table 1. Comparison of the performance of OP-IBBCEAS techniques reported in the literature
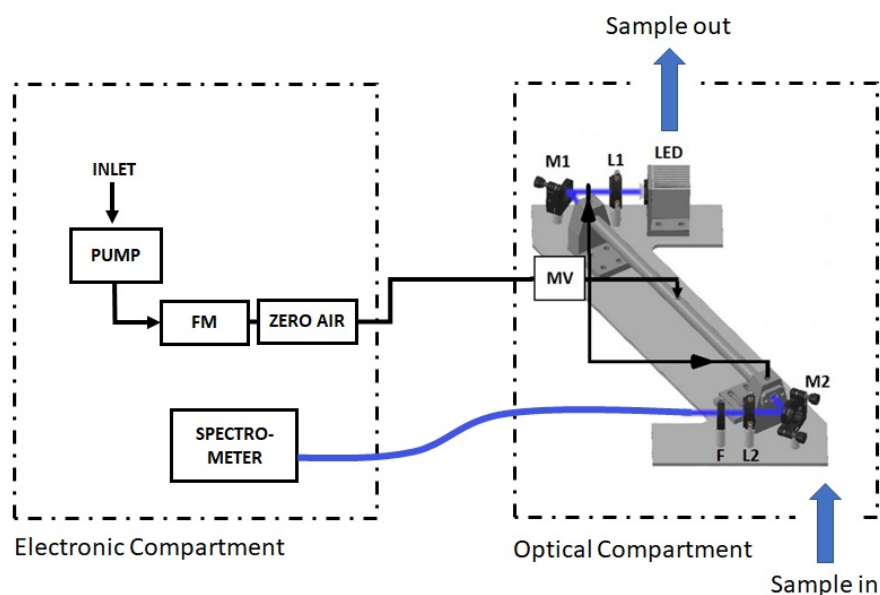
Figure 1. The OP-IBBCEAS setup. The optical components are separated from the rest of the setup, allowing the latter to be placed in a protected place while the optical part is exposed to external environmental conditions. The air coming from a diaphragm pump is pushed through a flow meter, FM and a Zero Air generator. A manual valve, MV, is used to control the flow. The flow is then split into three parts: one going to the centre of the cell tube and the other two used for purging the HR mirrors. The cell tube is mounted on a motorized translation stage for regularly acquiring spectra in absence of the absorbance. Details about the rest of the electronic components can be found in (Barbero et al., 2020).

2 Method

The IBBCEAS technique injects incoherent broad-band light into a high-finesse optical cavity for trace gas detection. The components used for this OP-IBBCEAS system are the same as those described in Barbero et al. (2020). The instrument uses a high-power LED (Luminus SBT70) centred at 445 nm with 19 nm FWHM (full width at half maximum) producing ~ 1 W of optical power cooled with a Peltier module (ET-161-12-08-E) and a fan–heat-sink assembly. A photodiode is placed perpendicular to the beam trajectory in the proximity of the collimating lens for monitoring the LED intensity overt time. The light from the LED is injected into a high-finesse optical cavity composed of two high-reflectivity mirrors (maximum reflectivity at 450 nm >99.990 $\pm$ 0.01 %; Layertec 109281). The radiation transmitted from the resonator is then focused on a bundle of seven optical fibres with 100 μm core diameter (FCRL-7UV100-2-SMA-FC) and sent to a spectrometer (Avantes AvaSpec-ULS2048L) composed of a diffraction grating (2400 lines mm^{-1}), a 2048-pixel charge-coupled device (CCD) and a 100 μm entrance slit. The resolution of the spectrometer was 0.54 $\pm$ 0.20 nm. In Barbero et al. (2020) the instrument was used in a close-path configuration and was mounted in a 19 in., 3U (5.25 in.) rack-mount case. In this current work, the optical part of the instrument, which was mounted on a Z-shaped 8-mm thick aluminium board, was displaced in a second

rack-mount case of the same size (Figures 1 and 2). The board was fixed on the rack using cylindrical dampers (Paulstra).
95   Underneath the board, four 5 W heating bands and one PT100 sensor were glued, and a RKC module (RF100) was used to regulate its temperature to minimize mechanical drift of the optical system due to ambient temperature fluctuations. A 16-cm inner diameter tube that on the close-path setup was used to flush the cavity with the air to be analysed was now mounted on a translation stage (Zaber, 001-X-LHM025A-KX13AF) for automatically displacing the tube in and out of the light beam. This allows to regularly inject zero air to measure the transmission from the cavity without the presence of absorption (I_0). One of
100 the two cavity mirror mounts was maid to be moved in and out along the axes of the cavity to switch between close path (CP) and OP configuration. In the case of the OP, the inner space between the two mirror mounts was a few millimetres larger than the tube. The gas connection was modified to use the diaphragm pump (KNF N 816 AV.12DC-B) to push the air through a filtering system (TEKRAN 90-25360-00 Analyzer Zero Air Filter). A total flow of 4 L min^{-1} STP was used for flushing the two cavity mirrors and the cavity tube with the inlet flow at the center and two outer flows at the edges of the tube ($\sim$1.3 L
105 min^{-1} at each channel). The optical box has a 70 cm^2 aperture at the front and air circulation is ensured by the fan system used for dissipating the heating of the LED assembly with an airflow capacity of $\sim$ 600 L min^{-1}. Sample air flow is therefore much higher than the zero air flow, minimizing the dilution on the sample flow provided by zero air flow. The rack was then placed in a plastic box (82 x 63 x 32 cm) with two aeration grids placed in front of the apertures at the front and back of the rack (Figure 2). The plastic box protects the instrument from bad weather conditions. At the air inlet and outlet, a plastic rainproof
110 ventilation grid with a plastic insect mesh net was installed, allowing to leave the instrument outside for long-term deployment. The two compartments can be installed 2m away from each other, allowing to keep the electronic-gas compartment inside a shelter while leaving the optical compartment outside.

For testing the performance of the OP-IBBCEAS instrument, the second IBB-CEAS configured in CP mode was used. The latter was calibrated using a laboratory system (FlexStreamTM Gas Standards Generator, KINTEK Analytical, Inc.) based on
115 a permeation tube of NO$_2$ (KIN-TEK ELSRT2W) which delivers known concentrations of NO$_2$. A calibration curve between 0 and 50 ppb of NO$_2$ was performed as described in Barbero et al. (2020). The OP system was first calibrated in CP configuration and then compared to the CP-IBBCEAS on indoor air measurements. All the errors reported in this work are expressed as 2σ.

3   Results

In Figure 3 we reported a typical spectrum recorded with the OP system during indoor and outdoor deployment. The signals
120 (Sp), fits, baselines (Bsln) and Residuals (Sp-Fit) of the fit are reported for the two cases. For indoor measurement, a baseline described by a polynomial of order 4 was sufficient to provide a flat residual, while for outdoor measurement the order was increased to 8. The fit results provided a concentration of $\sim$ 11 ppb of NO$_2$ in both cases. The spectra were obtained by averaging 200 spectra, for an acquisition time (t_{int}) of 24 sec (50 sec in total for acquiring I_0 and I signals) reaching a minimum absorption coefficient (α_{min}, corresponding to the standard deviation of the residuals) of 1.7 x 10^{-9} and 2.3 x
125 10^{-9} cm^{-1}, for indoor and outdoor measurement respectively. For outdoor measurements this corresponds to a figure of merit
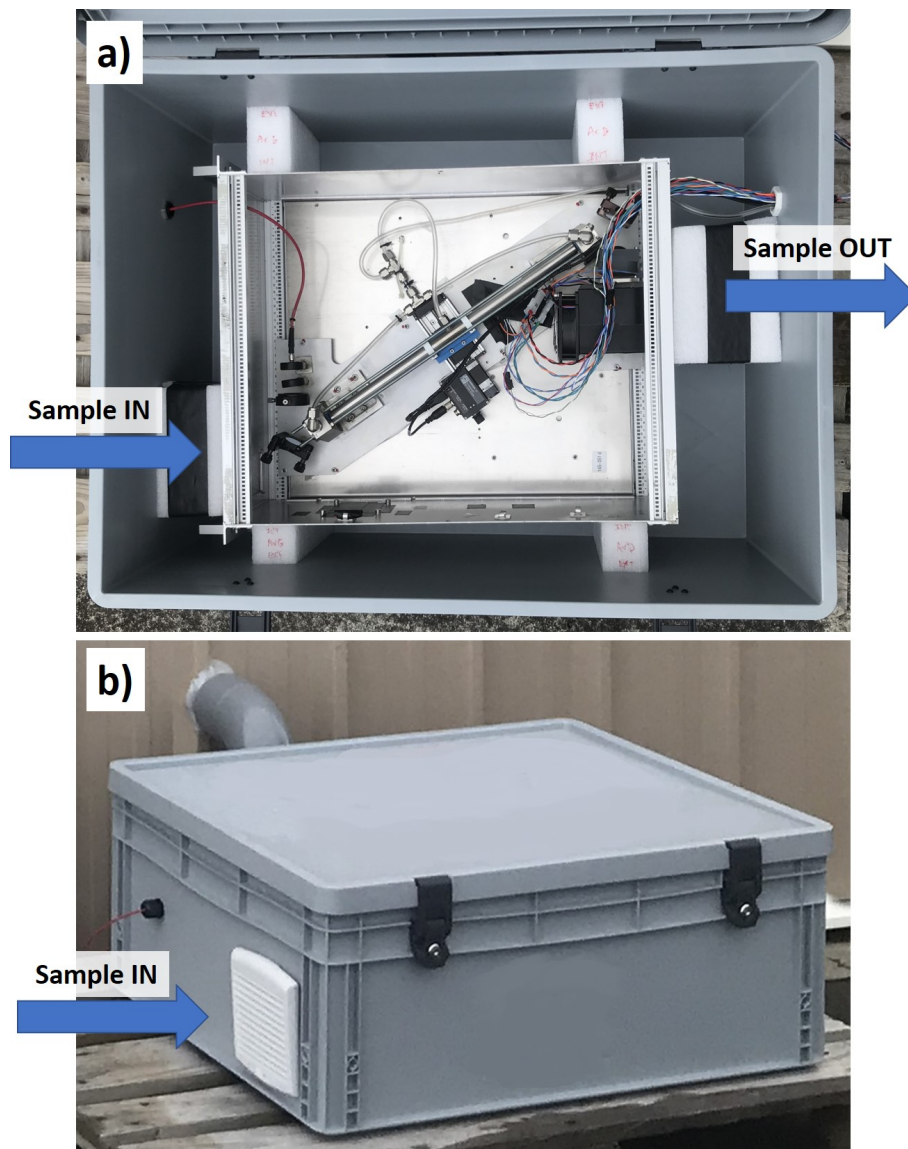
Figure 2. Pictures of the optical compartment. a) View inside the plastic box. The internal rack has a cover that was removed for the picture. b) the plastic box installed and ready for outdoor air measurements.

expressed as noise-equivalent absorption sensitivity (NEAS) or α_{min}(BW) = $\alpha_{min} \times (t_{int} / M)^{1/2}$ of 5.7×10^{-10} cm^{-1} Hz$^{-1/2}$ per spectral element (M).

The α_{min} was deduced for different time averages. The results are shown in the *log-log* plot of Figure 4, where the dots are the data and the dashed line indicates the trend in the case of a pure white-noise regime. Differently from the CP performances 130 reported in Barbero et al. (2020), here the performance deviates from the white-noise regime even at short time averages. From
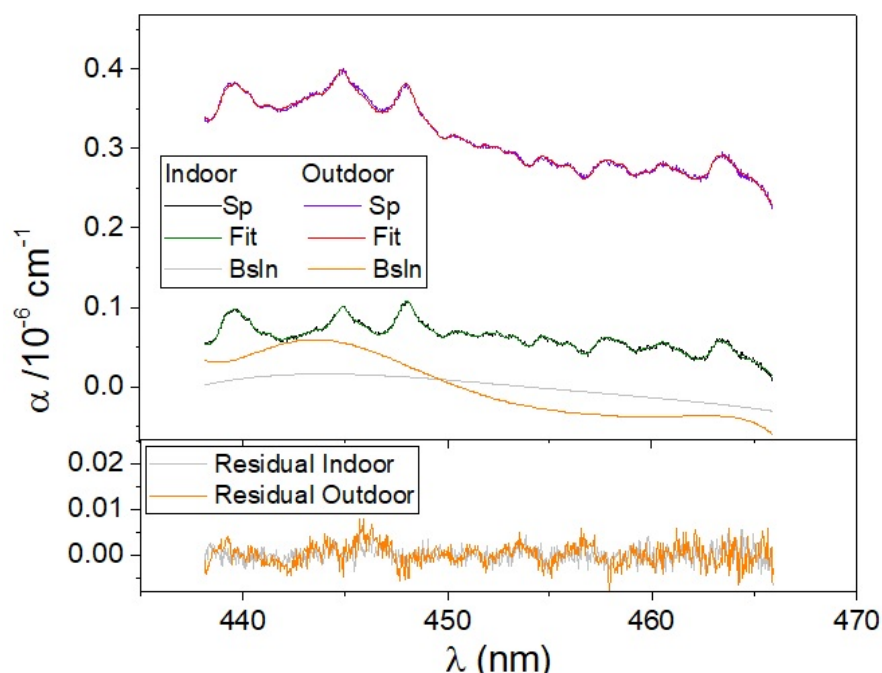
Figure 3. An example of the absorption spectra recorded with the OP-IBBCEAS instrument for indoor and outdoor measurements. The signal (in black and purple) and the fit (in green and red) are reported in the top panel together with the respective baselines (in grey and orange) described with a polynomial of order 4 and 8 for the indoor and outdoor case, respectively. At the bottom, the residuals of the fit (in grey and orange) were reported. The fit results provided a concentration of $\sim$11 ppb of NO_2 in both cases. The spectra were obtained by averaging 200 spectra, for an acquisition time of 24 sec (50 sec in total for acquiring I_0 and I signals) reaching a minimum absorption coefficient of 1.7×10^{-9} and 2.3×10^{-9} cm^{-1}, respectively.

this analysis one can see that the optimum integration time is $\sim$200 spectra (24 sec) and further integrating over time does not lead to a consistent reduction of the residuals.

A comparison of the measurements between the OP and the twin CP system was first conducted for indoor air. Both instruments were installed side-by-side in the laboratory with the inlet line of the CP system, a 2.5-m long ¼" PFA tube equipped
135 with a particle filter (Whatman®PTFE membrane filters – TE 38, 5 μm, 47 mm) placed as close as possible to the inlet aperture of the OP system. NO_2, IO and CHOCHO signals were monitored over 24 consecutive days and the results are reported in Figure 5. Good correlation between NO_2 measurements was observed with a slope of 0.9593 ± 0.0014 ($R^2 = 0.9957$, Figure 6). After the indoor comparison, the optical compartment of the OP instrument was moved outside, on the first-floor balcony of the IGE laboratory in Grenoble (45° 11′ 37.18″N, 5° 45′ 27.48″E, Saint Martin D'Hères, France). The gas inlet of the CP
140 instrument was placed again as close as possible to the inlet aperture of the OP system. Ten days of consecutive measurements were performed, and the results of the comparison are reported in Figure 5. Both instruments well captured the morning and evening peaks of NO_2 related to urban traffic. A discrepancy in the peak height was sometimes observed, particularly prior
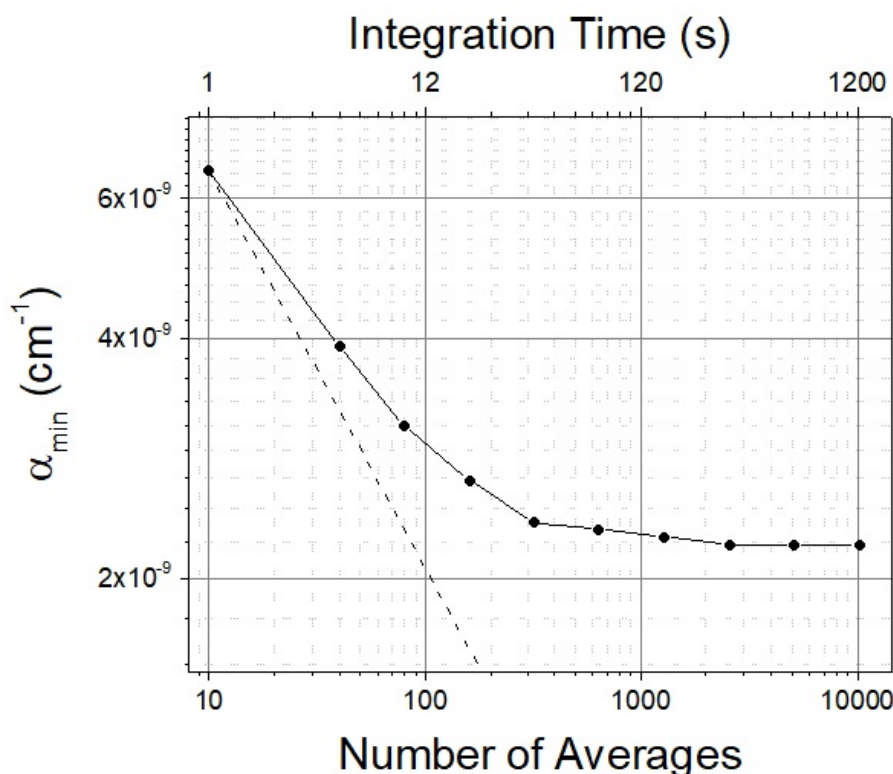
Figure 4. The minimum absorption coefficient α_{min} versus the number of spectral averages for the OP-IBBCEAS instrument. For these measurements, the instrument was installed in a pristine location to test the instrument in background conditions where NO_2 concentrations during the measurement period were ~ 0.55 ppb. Absorption spectra were averaged for different integration times, and α_{min} was calculated from the standard deviation of the residual.

October 8th at 12 am, but overall the two datasets showed a good correlation ($R^2 = 0.90$) with a slope of 0.8928 ± 0.005 R^2 = 0.9886 (or 0. 8717 $\pm$ 0.009, $R^2 = 0.9131$ if considering only data after October 8th at 12am, Figure 6). IO signal ranged

145 around zero for both instruments, with a mean of -0.09 $\pm$ 1.78 ppt for the CP and -0.29 $\pm$ 8.8 for the OP, with a degradation of the detection limit by a factor of 5 while operating in open-path conditions. Form CHOCHO mean values of -37.6 $\pm$ 108 and 388 $\pm$ 380 ppt for the CP and OP system were respectively observed during outdoor measurements highlighting the fact that the presence of the particle filter in the CP configuration lead to an underestimation of the concentrations of CHOCHO. This means that by comparing the two signals one can better constrain the presence of glyoxal in aerosol particles.

150 Due to the absorption of CHOCHO during outdoor measurements, the detection limit for the OP system was estimated using the indoor data. We estimated a precision of ± 7 ppt and $\pm$ 150 (pmol mol^{-1}, 2σ) in 50 seconds of measurement for IO and CHOCHO respectively. The small degradation in the precision of the IO to $\pm$ 8.8 ppt during the outdoor measurement can be explained by the presence of higher levels of NO_2. The precision on the NO_2 can be extrapolated to $\pm$ 150 ppt in 50 sec using the estimation for the CP reported in Barbero et al. (2020).
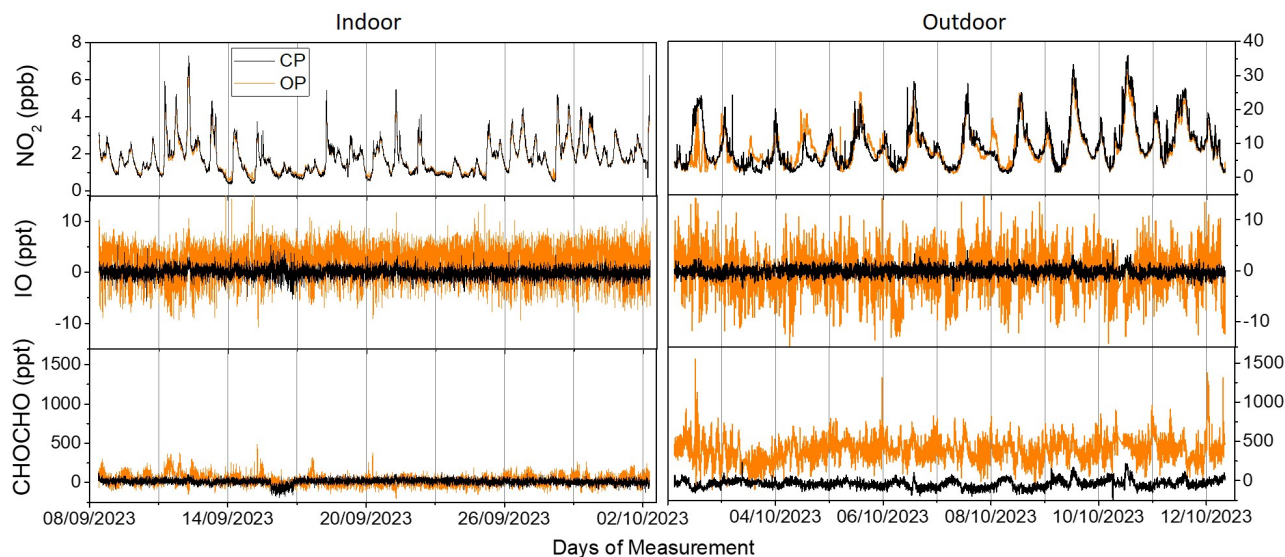
Figure 5. Left: 24-days comparison between close-path and open-path indoor air measurements using the two IBBCEAS instruments. The sample inlet of the close-path system was placed as close as possible to one of the open-path instruments. Mean values are -0.06 ± 1.96 and 2.26 ± 6.83 ppt for IO and -12.2 ± 67 and 29.7 ± 144 ppt (2σ) for CHOCHO for the CP and OP system, respectively. Right: 10-day comparison between close-path and open-path outdoor measurements conducted in Grenoble using the two IBB-CEAS instruments. The sample inlet of the close-path system was placed close to the open-path instrument. Mean values are -0.09 ± 1.78 and -0.29 ± 8.8 ppt for the IO and -37.6 ± 108 and 388 ± 380 ppt (2σ) for CHOCHO for the CP and OP system, respectively.

155   The dirtiness of the cavity mirrors is regularly monitored by the instrument. The average spectral intensity as well as the LED intensity are acquired every time the instrument records a spectrum in the absence of absorbance (I_0) and compared to the values stored during the latest calibration of the instrument. By monitoring both signals is possible to discriminate between a decrease in intensity of the LED source or a dirtiness of the cavity mirrors (leading to more intra-cavity losses and so to a lower transmission). During the 36 days of indoor and outdoor measurement reported in Figure 5 (Figure 3 for the

160   concentration records), the I_0 intensity signal (black) varied by few per cent, while the LED intensity (orange) varied 40 times less. This means that the variability observed at the cavity transmission does not depend on the performance of the LED. At the beginning of the experiment, the transmitted intensity was 5 % higher than during the instrument calibration. Furthermore, one can observe the sudden decrease by 2 % while installing the instrument outside, as well as the thermal effects on the mechanical stress of the instrument during the outdoor deployment, with an amplitude of the diurnal cycle of the spectrum

165   intensity of 1-2%. From this data monitoring we could confirm that during the 10-days continuous outdoor measurements, the open-path instrument did not experience degradation due to a possible dirtiness of the cavity mirrors. With this monitoring, the operator can have an idea of the properties of the cavity mirrors, and decide when is time to interrupt the measurement to clean them. In the context of a continuous laser injection of light into a resonator composed of two identical mirrors of reflectivity R, the ratio between the light intensity at the output of the cavity, denoted here as I_{out}, and the injected intensity, denoted here
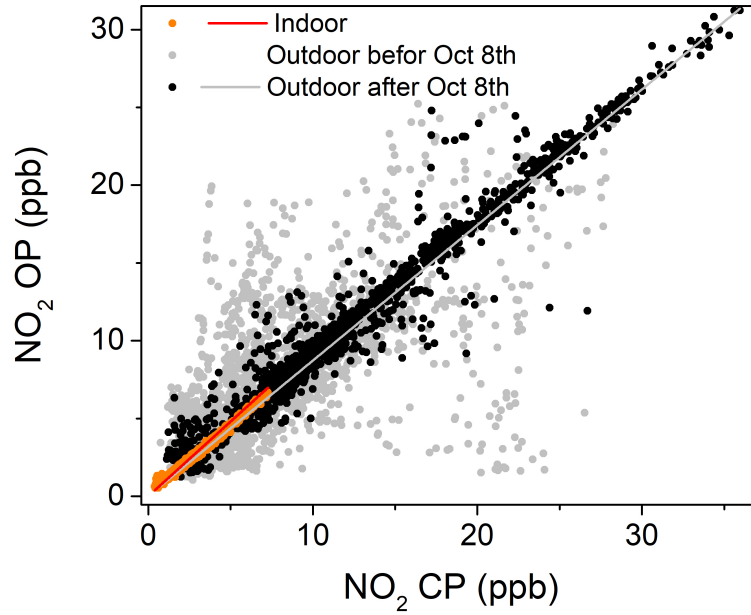
Figure 6. Linear correlations between the NO_2 measured by the OP and the CP were obtained for both indoor and outdoor measurements. Due to the sometimes observed discrepancy in the peak height, particularly prior October 8th at 12 am, the dataset was separated in two, prior October 8th at 12am (grey) with more scattered data and after (in black) for outdoor measurement. The latter was used for the linear regression, with slopes of 0.9593 ± 0.0014 ($R^2 = 0.9957$) and 0.8928 ± 0.005 ($R^2 = 0.9886$) obtained for indoor and outdoor measurements, respectively. Both intercepts were forced to zero.

170   as I_{in}, is expressed through the following equation:

$$I_{out} = I_{in}((1-R)^2(1-A))/(1-R^2((1-A))^2) \tag{1}$$

Where A is the absorption inside the cavity. In our case we are monitoring the change in intensity in the absence of absorption, so eq 1 can be simplified as follow:

$$I_{out} = I_{in}(1-R)/(1+R) \tag{2}$$

175   So, for high reflective mirrors ($R \longrightarrow 1$) we can say that the relative change in intensity is directly proportional to (1-R) which is the inverse of the enhancement factor on the effective optical path-length (L_{eff}) provided by a resonator of length L:

$$I_{out}/I_{in} \propto 1 - R = L/L_{eff} \tag{3}$$

Mechanical instabilities play an important role here. A small misalignment of the cavity may lead to a change in the relative intensity of the light transmitted even if the mirror's reflectivity did not change. Therefore, the operator must regularly assess
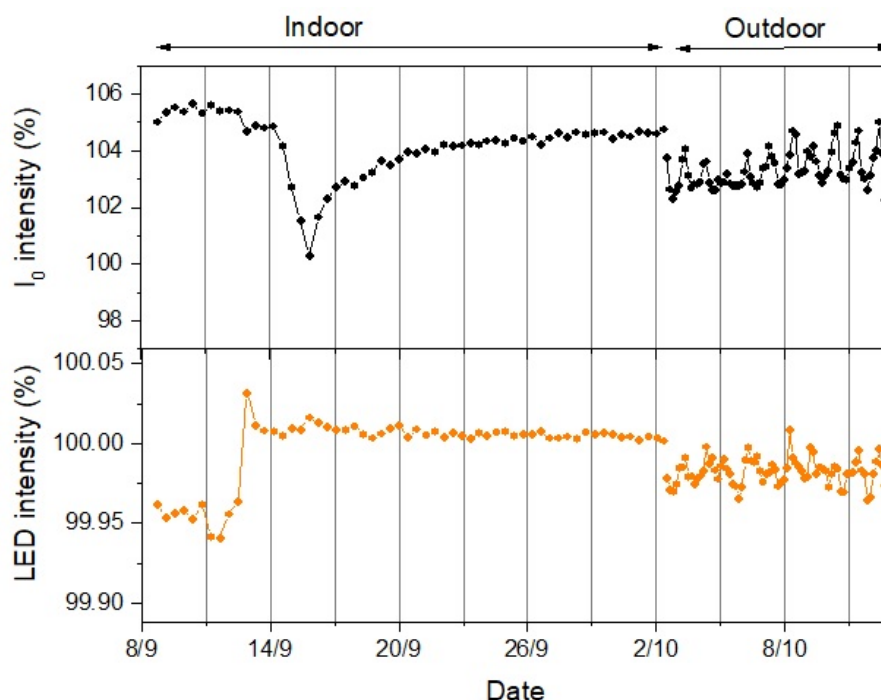
Figure 7. Average spectrum intensity (top) and LED intensity (bottom) recorded during I_0 measurements for indoor and outdoor measurements and expressed as a percentage with respect to the values registered during the calibration of the instrument prior the measurements.

180 the relative variation in intensity over time from the moment the instrument is installed. The frequency of this monitoring should be adapted to the quality of the air of the environment, with weekly monitoring in urban areas and monthly in more remote environments.

4   Conclusions

In this work, we reported the development of an open-path IBB-CEAS (Incoherent Broad-Band Cavity Enhanced Absorbtion
185 Spectroscopy) system for simultaneous measurement of NO_2, IO and CHOCHO. The instrument is equipped with an automatized system allowing to regularly acquire spectra in the absence of absorption. By purging the cavity mirrors with filtered dry air, we proved a continuous operation for up to 10 days without observing a degradation of the mirror reflectivity. We compared the performance between the closed-path (CP) and open-path (OP) configurations and compared the instrument during long-term indoor and outdoor surveys. The system is light ($\sim$ 20 kg for the two racks), compact, robust and easy to install in
190 the field, with a power consumption of < 300 W. A similar development can be used in the future to measure other atmospheric interest radicals such as the other XO and OXO molecules, but also HO, HO_2 and RO_2 using different light sources in the UV, Visible and infrared region and with the respective high-reflective mirrors and optical spectrometers.

Author contributions. The development was ideated by RG and conducted by FP and RG under the supervision of RG. Data analysis were conducted by FP and RG. NC contributed to the deployment of the system. JS is the leader of the CAPOXI 35–75 project. The paper was
195 written by FP and RG, with contributions from all authors.

Competing interests. The authors declare no conflict of interest.

Acknowledgements. This work was supported by the French Polar Institute (IPEV) through programs 1177 (CAPOXI 35–75) and by the Scientific Grant Agency of the Slovak Republic VEGA 1/0710/24. The authors would like to thank Jack Saville and Guillaume Méjean for carefully reading and checking the manuscript.

References

Barbero, A., Blouzon, C., Savarino, J., Caillon, N., Dommergue, A., and Grilli, R.: A compact incoherent broadband cavity-enhanced absorption spectrometer for trace detection of nitrogen oxides, iodine oxide and glyoxal at levels below parts per billion for field applications, Atmospheric Measurement Techniques, 13, 4317–4331, https://doi.org/10.5194/amt-13-4317-2020, 2020.

Beynon, W. and Williams, E.: The long term variation in the ionospheric winter absorption anomaly, Journal of Atmospheric and Terrestrial Physics, 38, 423–429, https://doi.org/10.1016/0021-9169(76)90069-6, 1976.

Dixneuf, S., Ruth, A., Häseler, R., Brauers, T., Rohrer, F., and Dorn, H.-P.: Comparison of nitrous acid detection using open-path incoherent broadband cavity-enhanced absorption spectroscopy and extractive long-path absorption photometry, Meas. Tech, 291, 1–28, https://doi.org/10.5194/amt-15-945-2022, 2021.

Dixneuf, S., Ruth, A., Häseler, R., Brauers, T., Rohrer, F., and Dorn, H.: Detection of nitrous acid in the atmospheric simulation chamber SAPHIR using open-path incoherent broadband cavity-enhanced absorption spectroscopy and extractive long-path absorption photometry, Atmospheric Measurement Techniques, https://doi.org/10.5194/amt-15-945-2022, 2022.

Fanhao, M., Min, Q., Wu, F., Jun, D., Ke, T., Helu, Z., dou, S., Zhitang, L., and Pinhua, X.: Measurements of atmospheric HONO and NO2 utilizing an open-path broadband cavity enhanced absorption spectroscopy based on an iterative algorithm, Acta Physica Sinica, https://doi.org/10.7498/aps.71.20220150, 2022.

Gómez Martín, J. C., Lewis, T. R., Blitz, M. A., Plane, J. M., Kumar, M., Francisco, J. S., and Saiz-Lopez, A.: A gas-to-particle conversion mechanism helps to explain atmospheric particle formation through clustering of iodine oxides, Nature communications, 11, 4521, https://doi.org/10.1038/s41467-020-18252-8, 2020.

Grilli, R., Méjean, G., Kassi, S., Ventrillard, I., Abd-Alrahman, C., and Romanini, D.: Frequency comb based spectrometer for in situ and real time measurements of IO, BrO, NO2, and H2CO at pptv and ppqv levels, Environmental science & technology, 46, 10 704–10 710, https://doi.org/10.1021/es301785h, 2012.

Hönninger, G., Von Friedeburg, C., and Platt, U.: Multi axis differential optical absorption spectroscopy (MAX-DOAS), Atmospheric Chemistry and Physics, 4, 231–254, https://doi.org/10.5194/acp-4-231-2004, 2004.

Nasse, J.-M., Eger, P. G., Pöhler, D., Schmitt, S., Frieß, U., and Platt, U.: Recent improvements of long-path DOAS measurements: impact on accuracy and stability of short-term and automated long-term observations, Atmospheric Measurement Techniques, 12, 4149–4169, https://doi.org/10.5194/amt-12-4149-2019, 2019.

Romer Present, P. S., Zare, A., and Cohen, R. C.: The changing role of organic nitrates in the removal and transport of NOx, Atmospheric Chemistry and Physics, 20, 267–279, https://doi.org/10.5194/acp-20-267-2020, 2020.

Saiz-Lopez, A., Blaszczak-Boxe, C. S., and Carpenter, L.: A mechanism for biologically induced iodine emissions from sea ice, Atmospheric Chemistry and Physics, 15, 9731–9746, https://doi.org/10.5194/acp-15-9731-2015, 2015.

Simpson, W. R., Brown, S. S., Saiz-Lopez, A., Thornton, J. A., and von Glasow, R.: Tropospheric halogen chemistry: Sources, cycling, and impacts, Chemical reviews, 115, 4035–4062, https://doi.org/10.1021/cr5006638, 2015.

Suhail, K., Suhail, K., George, M., Chandran, S., Chandran, S., Varma, R., Venables, D., Wang, M., and Chen, J.: Open path incoherent broadband cavity-enhanced measurements of NO3 radical and aerosol extinction in the North China Plain., Spectrochimica acta. Part A, Molecular and biomolecular spectroscopy, 208, 24–31, https://doi.org/10.1016/j.saa.2018.09.023, 2019.

Varma, R. M., Venables, D. S., Ruth, A. A., Heitmann, U., Schlosser, E., and Dixneuf, S.: Long optical cavities for open-path monitoring of atmospheric trace gases and aerosol extinction, Applied optics, 48, B159–B171, 2009.

Volkamer, R., San Martini, F., Molina, L. T., Salcedo, D., Jimenez, J. L., and Molina, M. J.: A missing sink for gas-phase glyoxal in Mexico City: Formation of secondary organic aerosol, Geophysical Research Letters, 34, https://doi.org/10.1029/2007GL030752, 2007.

Wang, H. and Lu, K.: Monitoring Ambient Nitrate Radical by Open Path Cavity Enhanced Absorption Spectroscopy., Analytical chemistry, https://doi.org/10.1021/acs.analchem.9b01971, 2019.

Wang, M., Lou, S., Hu, W., Wang, H., Wang, X., Fan, F., Varma, R., Venables, D., and Chen, J.: Intercomparison of NO3 under Humid Conditions with Open-Path and Extractive IBBCEAS in an Atmospheric Reaction Chamber, Remote. Sens., 15, 739, https://doi.org/10.3390/rs15030739, 2023.

Wu, T., Wu, T., Chen, W., Fertein, E., Cazier, F., Dewaele, D., and Gao, X.: Development of an open-path incoherent broadband cavity-enhanced spectroscopy based instrument for simultaneous measurement of HONO and NO2 in ambient air, Applied Physics B, 106, 501–509, https://doi.org/10.1007/S00340-011-4818-3, 2012.